Nonlinear Control for Joint Air and Fuel Management in a SI Engine

Jun-Mo Kang and J. W. Grizzle
Department of Electrical Engineering and Computer Science
University of Michigan, Ann Arbor, MI 48109-2122
{junmo,grizzle}@eecs.umich.edu

Abstract

Engines equipped with a means to actuate air flow at the intake port can achieve superior fuel economy performance in steady state. This paper shows how modern nonlinear design techniques can be used to control such an engine over a wide range of dynamic conditions. The problem is challenging due to the nonlinearities and delays inherent in the engine model, and the saturation of the air flow actuator. The control solution has two novel features. Firstly, a saturation recovery method is directly integrated into the nonlinear control design. The second novel feature is that the control Lyapunov function methodology is applied to a discrete-time model. The performance of the controller is evaluated and compared with a conventionally controlled engine through simulations.

1 Introduction

In the design of an engine controller, one must optimize and make tradeoffs between fuel economy, drivability (torque management) and emissions. Since an automobile must meet stringent federal emissions regulations in order to be sold, emissions control often is the most important factor. The customer, however, will consider fuel economy and torque response in making a selection.

The three way catalytic converter is the current technology for meeting emissions regulations. When operated near the stoichiometric point, emission conversion efficiencies of 98 % for hydrocarbons, carbon monoxide and oxides of nitrogen can be achieved. However, as seen in Figure 1, deviations of ± 0.2 air fuel ratio (A/F) will cause the conversion efficiency of at least one of the emission components to drastically decrease. Thus an important control objective is to maintain the air fuel ratio near stoichiometry.

In a standard spark ignition engine, the primary actuator is the fuel injector, which is typically located at the intake port. The mass flow rate of air entering the intake manifold is measured with a hot wire anemometer, and the fuel injected into the engine is adjusted to achieve a stoichiometric mixture; this is clearly a feedforward control action. In order to compensate for inevitable errors in A/F, the A/F is measured in the exhaust stream with an exhaust gas oxygen (EGO) sensor, and a PI feedback control loop is then used to achieve zero steady state error for constant throttle position and engine speed.

Extensive research has been done to improve A/F control performance of the system. Part of this research has focused on accurate estimation of transient air flow, thereby improving the accuracy of the feedforward controller. Another possibility is to control the air flow into the intake manifold with an electronic throttle [5, 13], or

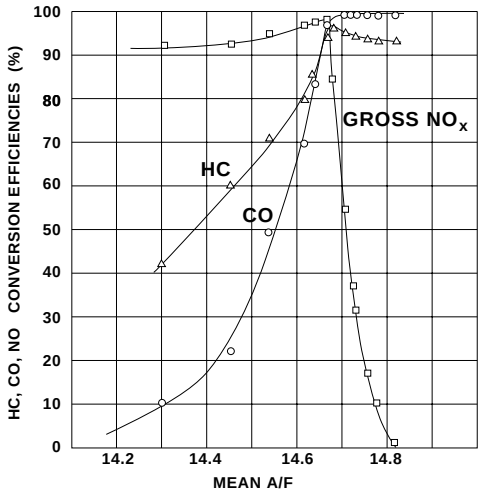

Figure 1: Steady state conversion efficiency of TWC.

the air flow into the cylinders. This latter actuation can be achieved by adjusting the cam timing of the intake valves [1], by implementing independent electro-hydraulically controlled intake valves [6], by secondary (or port) throttles [7], or by using secondary valves in series with conventional intake valves [10]. The common element of these actuators is that they allow control of the air flow into the cylinders by adjusting the effective area of intake valves. Three of these methods, namely variable intake cam timing, variable intake valve control, and series secondary valves can also be used to improve fuel economy. This is because, by controlling the breathing process of the engine, it is possible to raise the average manifold pressure, and thereby reduce pumping losses in the engine [6, 10].

The local aspects of joint air and fuel control have been studied in [7] by designing a linear controller based around a specific operating point. The torque (drivability) and A/F responses were superior or equal to that of a conventional engine (with fuel PI control) for small step changes in the primary throttle position. The major problem encountered with the linear analysis was that the resulting closed-loop system went unstable for large changes in the primary throttle position. This can be traced to two causes: the nonlinearities in the engine model and saturation in the air flow actuator.

This paper will attempt to address these issues by developing a more global control strategy based on control Lyapunov functions (clf). This design has two novel features. Firstly, a saturation recovery method is directly integrated into the nonlinear control design. The basic idea is to make the reference signal track the actual output of the system whenever saturation occurs, thereby avoiding integrator windup. The second novel feature is that the clf method-

ology is applied to a discrete-time model. The performance of the controller is evaluated and compared with the conventionally controlled engine through simulations.
An overview of the engine model used in this study is presented in the next section. Control objectives are summarized in Section 3. The nonlinear control design is carried out in Section 4. Simulations are presented in Section 5.

2 Engine Model

2.1 Conventional model

The basic engine representation used here is the well-known model of [3]. This is a nonlinear, continuous-time, mean-valued, phenomenological representation of a conventional, port-fuel injected, spark ignition, 2.0 L, 4-cylinder, gasoline engine. The dynamic model of the intake manifold is based on the "Filling and Emptying model" described in [2]. In this approach, the manifold is regarded as a plenum with a constant volume, where the rate of change of the manifold pressure (P_m) is proportional to the difference between the mass air flow rate into the manifold ($\dot{m}_\theta$) and that pumped out of the manifold into the cylinders ($\dot{m}_{cyl}$). This relation is expressed as a first order differential equation,

$$\frac{d}{dt}P_m = K_m(\dot{m}_\theta - \dot{m}_{cyl}) \tag{1}$$

where $K_m = \frac{R \cdot T_m}{V_m}$, R is the specific gas constant, T_m is the manifold temperature, and V_m is the manifold volume. The mass air flow rate into the intake manifold through the throttle body is a function of the primary throttle angle (θ), the upstream or ambient pressure (P_o) and the downstream pressure, which is manifold pressure. Upstream pressure is assumed to be atmospheric (i.e., P_o= 1 bar):

$$\begin{aligned} \dot{m}_\theta &= f(\theta)g(P_m) \\ f(\theta) &= 2.821 - 0.05231\theta + 0.10299\theta^2 - 0.00063\theta^3 \\ g(P_m) &= \begin{cases} 1 & \text{if} \quad P_m \le P_o/2 \\ \frac{2}{P_o}\sqrt{P_m P_o - P_m^2} & \text{if} \quad P_m > P_o/2 \end{cases} \end{aligned} \tag{2}$$

In a conventional engine, the mass air flow rate into the cylinders ($\dot{m}_f$) is a function of manifold pressure and engine speed (N), and for the engine under study is given by

$$\begin{aligned} \dot{m}_f = \quad & -0.366 + 0.08979N \cdot P_m - 0.0337N \cdot P_m^2 \\ & +0.0001N^2 \cdot P_m \end{aligned} \tag{3}$$

The discrete-event nature of the combustion process introduces transport delays, which are dependent on engine speed. This motivates discretizing the overall model synchronously with engine events [8, 9]. That is, the independent variable is transformed from time to crank-angle, and the model is then discretized at a constant rate in the crank-angle domain. Here, the model is discretized with period π radians in crank-angle, which corresponds to one engine event (elapsed time or revolution for the intake stroke, for example). This procedure introduces speed dependent terms in the dynamics, but it permits standard stability analysis to be applied.
The calculation delay in the injection of fuel and the transport delays between the exhaust manifold and the EGO sensor are included in the model. The dynamics of the EGO sensor is modeled by a first order difference equation; in the time domain, its time constant is 0.20 sec.
The steady state engine brake torque is affected by many parameters such as ignition delay, EGR and so on. The general relations between these parameters and brake torque are derived from experimental data and curve fitting methods [8]:

$$\begin{aligned} T_b = \quad & -181.3 + 379.36m_a + 21.91A/F - 0.85A/F^2 \\ & +0.26\sigma - 0.0028\sigma^2 + 0.027N - 0.000107N^2 \\ & +0.00048N\sigma + 2.55\sigma m_a - 0.05\sigma^2 m_a + 2.36\sigma m_e \end{aligned} \tag{4}$$

where

m_a	:	mass air charge (g/intake event)
A/F	:	air-fuel ratio
N	:	engine speed (rad/sec)
m_e	:	EGR (g/intake event)
σ	:	degrees of spark advance before top dead center

For simplicity in this study, it is assumed that there is no EGR (i.e., m_e=0) and ignition delay (σ) is set to 30°.
The above model was identified [3] at air fuel ratios between 13.6 and 15.6, engine speeds between 80 rad/sec and 625 rad/sec, manifold pressures between 0.35 to 1.0 in bar, and torque from 14 to 135 Nm.

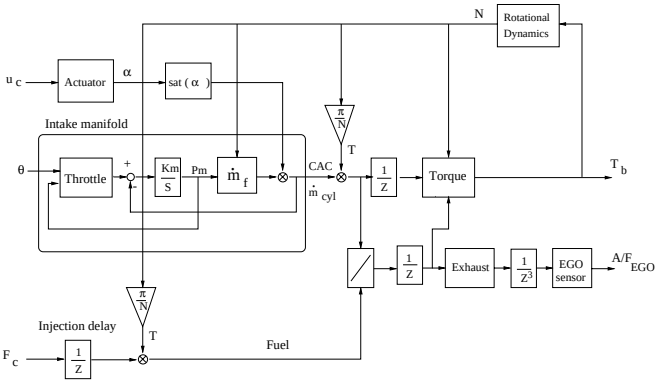

Figure 2: Nonlinear hybrid engine model.

2.2 Cylinder air charge control

To account for the actuation of the cylinder air charge, the flow rate into the cylinders is modified as

$$\dot{m}_{cyl} = \alpha \cdot \dot{m}_f \tag{5}$$

where α represents the normalized effective area of the intake valves, and is limited between 0 and 1. Depending on the actuation scheme used, more or less manipulation may be necessary to put the model in this form. However, each scheme has the qualitative feature of being able to increase or decrease the air admitted into the cylinder, over a certain range.
On a practical basis, the choice of the particular air charge actuation scheme will be based on many factors. For example, in the view of fuel economy, control of the cylinder air charge via intake valve timing or intake valve open duration reduces pumping losses by allowing increased intake port pressure, which is essentially equivalent to intake manifold pressure [6]. On the other hand, secondary throttles choke the air flow at the intake ports, thereby decreasing the intake port pressure, which results in increased pumping losses [2]. Other issues such as reliability and cost must also be considered. The analysis carried out in this paper is valid for any actuation scheme that can be modeled by (5).
From the control point of view taken in this paper, the primary difference between the various schemes lies in the speed of response

of the associated actuator dynamics. For definiteness, this paper assumes a hydraulic actuator with a time constant $\tau_a = 0.001$. When discretized on an engine-event basis, the model is

$$\alpha(k+1) = (1 - \frac{\pi}{N\tau_a})\alpha(k) + \frac{\pi}{N\tau_a}u_c(k) \quad (6)$$

3 Control Problem Description

The major objectives of the control design are:

1. exploit the air flow actuation capability to achieve higher manifold pressure, thereby reducing pumping losses and improving fuel economy;
2. achieve a torque response that is as similar as possible to a conventional engine so that there is no perceptible loss in drivability;
3. minimize A/F excursions from stoichiometry to maximize the simultaneous conversion efficiency of the catalyst, thereby minimizing overall emissions.

The control inputs are intake valve effective area and (amount of) fuel injection. It is assumed that the A/F is measured by a linear EGO sensor placed in the exhaust stream, just ahead of the catalyst. In addition, it is assumed that some means of measuring torque is available.

As stated, the problem has two-inputs, two-measured outputs and three performance objectives. This imbalance is treated by "squaring down" the performance objectives. At stoichiometry, torque depends primarily on mass air flow. At low primary throttle angle, a static mass air flow model is constructed so as to closely match the steady state torque of the joint-air-and-fuel-controlled engine to that of the conventional engine, while maintaining the intake manifold pressure greater than 0.5 bar, in steady state. This also guarantees control authority over cylinder mass air flow rate [1]; see Figure 3. In this regime, the effective intake valve area is near 0.5 to 0.6. At high primary throttle angles, the manifold pressure is already high in a conventional engine, and hence, the static mass air flow model is simply designed to closely match the steady state torque of the conventional engine.

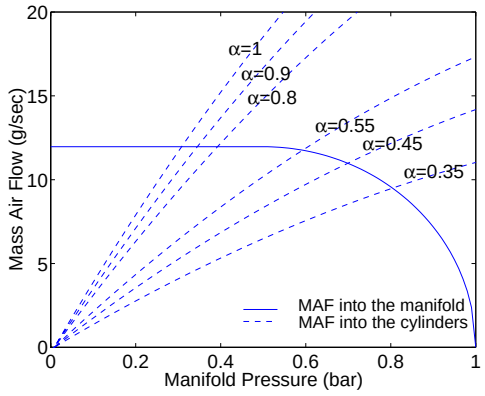

Figure 3: Steady state MAF corresponding to the effective intake valve area at a primary throttle angle of 10°, and an engine speed of 300 rad/sec.

The static mass air flow model, and hence the static torque model as well, is a function of the primary throttle angle and engine speed. The control problem is now defined as in Figure 4: the objective is to design a controller that achieves zero steady state error in commanded torque and stoichiometric A/F for constant throttle inputs. The commanded torque is taken to be a low pass

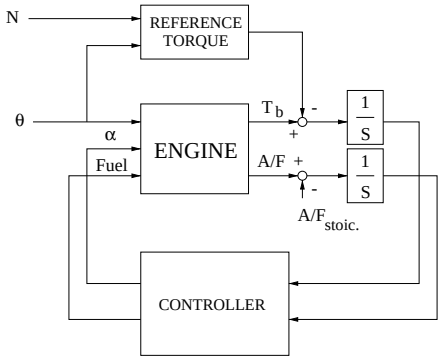

Figure 4: Control structure.

filtered version of the static torque model. The time constant, τ_r is to be adjusted to trade off drivability (speed of torque response) with emissions (deviations in A/F from stoichiometry).

$$\begin{aligned} x_r(k+1) &= (1 - \tfrac{\pi}{N\tau_r})x_r(k) + \tfrac{\pi}{N\tau_r}u_r(k) \\ u_r(k) &= T_{b,static}(N,\theta) \\ T_{b,ref} &= x_r(k) \end{aligned} \quad (7)$$

4 Nonlinear Feedback Control based on Control Lyapunov Functions

This section follows a recent approach to the design of nonlinear controllers, namely control Lyapunov functions (clf) and backstepping [11, 12, 14]. A nonlinear feedback controller for the torque and feedgas portion of the system shown in Figure 5 is developed based on a positive semi-definite clf. The controller for a simplified version of this model is investigated first, and then the result is extended to the full order model. Finally, the resulting control law is back stepped through the actuator dynamics to obtain the final result.

One of the novelties in this work is the use of control Lyapunov functions on a discrete-time system model. Most of the work in this area has focused on continuous-time models.

4.1 State feedback control for torque and feedgas model

In this subsection and the next, the potential saturation of the air flow actuator is ignored. This will be remedied in Subsection 4.3. The torque and feedgas model in Figure 5 includes delays and nonlinearities (air-fuel division and torque generation). To aid in the feedback design, the torque generation equation (4) is linearized around stoichiometry, resulting in

$$\begin{aligned} T_b = \; & 410.86m_a - 2.98(A/F - A/F_{stoic.}) - 37.44 \\ & + 0.0414N - 0.000107N^2 \end{aligned} \quad (8)$$

Figure 6 shows that approximation error is less than 1 Nm for air fuel ratios between 13.6 and 15.6, where the nonlinear model is identified.

To fix the main ideas of the clf design, a simplified version of the model plus integrators is studied first, as shown in Figure 7. The

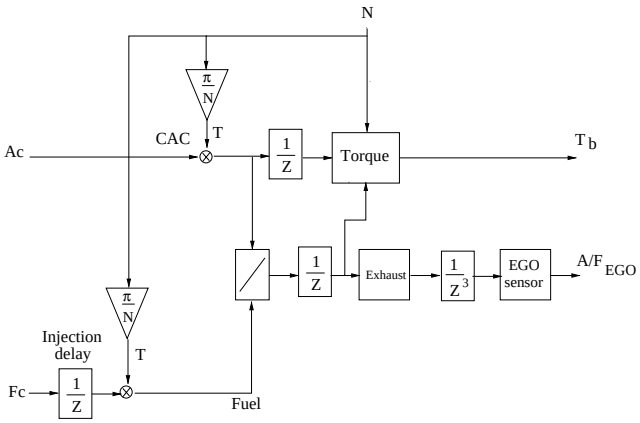

Figure 5: Torque and feedgas portion of the engine model.

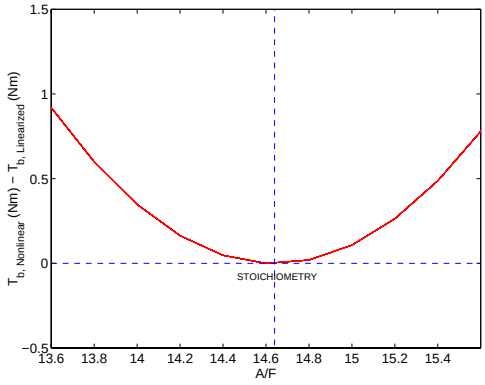

Figure 6: Torque error between nonlinear and linearized model given MAF and engine speed.

control signal ΔF is defined as the inverse (amount of) fuel to inject (i.e., $\Delta F = \frac{1}{F_c}$). The state equations are given by

$$\begin{array}{lcl} x_1(k+1) & = & \Delta F \\ q_1(k+1) & = & q_1(k) + \frac{\pi}{N}(T_b - T_{b,ref}) \\ & = & q_1(k) + \frac{\pi}{N}(\delta(N) - T_{b,ref} + 410.86T\Delta A \\ & & -2.98(x_1(k)\Delta A - A/F_{stoic.})) \\ q_2(k+1) & = & q_2(k) + \frac{\pi}{N}(A/F_{EGO} - A/F_{stoic.}) \\ & = & q_2(k) + \frac{\pi}{N}(x_1(k)\Delta A - A/F_{stoic.}) \end{array} \quad (9)$$

where

$T_{b,ref}$: brake reference torque (Nm)

T : intake event duration, $\frac{\pi}{N}$ (sec)

$\delta(N) = -37.44 + 0.0414N - 0.000107N^2$

Since $q_1(k+1)$ and $q_2(k+1)$ have common terms, it is natural to choose a candidate Lyapunov function as

$$V_{L1}(k) = V_1^2(k) = (q_1(k) + 2.98q_2(k))^2 \quad (10)$$

so that these two states are bounded relative to each other; that is, if one of them is bounded, then so is the other. The difference equation of this Lyapunov function is given by

$$\begin{array}{l} V_{L1}(k+1) - V_{L1}(k) \\ = (V_1(k+1) - V_1(k))(V_1(k+1) + V_1(k)) \\ = \frac{\pi}{N}(410.86T\Delta A + \delta(N) - T_{b,ref})(V_1(k+1) + V_1(k)) \end{array} \quad (11)$$

Choosing the control law as

$$\Delta A = \frac{1}{410.86T}(T_{b,ref} - \delta(N) - c_1\frac{N}{\pi}V_1(k)) \quad (12)$$

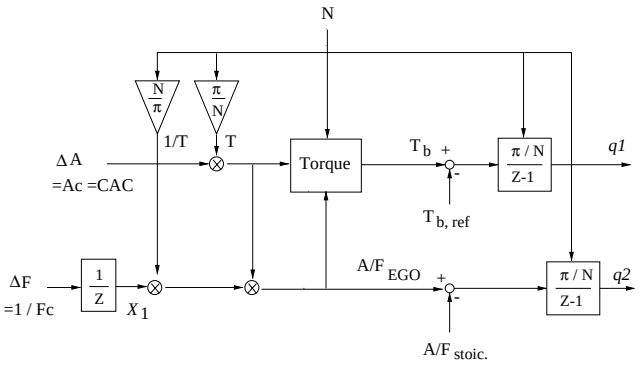

Figure 7: Simplified version of torque and feedgas model.

with appropriate gain c_1 results in

$$V_1(k+1) - V_1(k) = -c_1V_1(k) \quad (13)$$

and makes the difference equation of Lyapunov function V_{L1} negative semi-definite:

$$V_{L1}(k+1) - V_{L1}(k) = -c_1(2-c_1)V_1^2(k) \quad (14)$$

In the next step, another candidate Lyapunov function with parameter K is chosen to force one of the integral states, q_2, to be bounded relative to the state x_1:

$$V_{L2}(k) = V_2^2(k) = (Kq_2(k) + x_1(k))^2 \quad (15)$$

Thus, if it can later be proven that any one of x_1, q_1 or q_2 is bounded, then all of them are. The difference equation of Lyapunov function V_{L2} is given by

$$\begin{array}{l} V_{L2}(k+1) - V_{L2}(k) \\ = (V_2(k+1) + V_2(k))(V_2(k+1) - V_2(k)) \\ = (V_2(k+1) + V_2(k))(K\frac{\pi}{N}(x_1(k)\Delta A - A/F_{stoic.}) \\ \quad + \Delta F - x_1(k)) \end{array} \quad (16)$$

Choosing the control law with appropriate gain c_2

$$\Delta F = -K\frac{\pi}{N}(x_1(k)\Delta A - A/F_{stoic.}) + x_1(k) - c_2V_2(k) \quad (17)$$

results in

$$V_2(k+1) - V_2(k) = -c_2V_2(k) \quad (18)$$

and makes the difference equation of Lyapunov function V_{L2} negative semi-definite:

$$V_{L2}(k+1) - V_{L2}(k) = -c_2(2-c_2)V_2^2(k) \quad (19)$$

A composite, positive semi-definite Lyapunov function for the simplified version of the torque and feedgas model is given by

$$V_L(k) = V_{L1}(k) + V_{L2}(k) = V_1^2(k) + V_2^2(k) \quad (20)$$

Then the difference equation of Lyapunov function V_L with inputs (12) and (17) becomes negative semi-definite

$$V_L(k+1) - V_L(k) = -c_1(2-c_1)V_1^2(k) - c_2(2-c_2)V_2^2(k) \quad (21)$$

The goal now is to understand what (21) implies about the stability of the model (9). When V_{L1} and V_{L2} are both equal to zero, the control signals become

$$\begin{array}{ll} \Delta A \longrightarrow & \frac{T_{b,ref} - \delta(N)}{410.86T} \\ \Delta F \longrightarrow & (1 - K\frac{\pi}{N}\frac{T_{b,ref} - \delta(N)}{410.86T})x_1(k) + K\frac{\pi}{N}A/F_{stoic.} \end{array} \quad (22)$$

The parameter K is now chosen so that x_1 is stabilized with (22):

$$|1-K\frac{\pi}{N}\frac{T_{b,ref}-\delta(N)}{410.86T}|<1 \tag{23}$$

Under this condition, the states of (9) are asymptotically stable conditionally to the largest positively invariant set contained in $Z=\{x|V_L(x)=0\}$, [11]. By Theorem 2.24 of [11] (the discrete-time version of the theorem and its proof are given in the Appendix), the states of (9) are bounded, and thus by LaSalle's Theorem [15], they approach the largest positively invariant set contained in $W=\{x|\Delta V_L(x)=0\}$. From (20) and (21), $W=Z$. From these facts, it follows that the control signals converge to (22), and consequently, the states converge to constant values. This then gives that the steady state torque and A/F errors are zero.
For the full order model, the state equations are

$$\begin{array}{lcl}
x_1(k+1) & = & T\Delta A \\
x_2(k+1) & = & \Delta F \\
x_3(k+1) & = & \Delta A x_2(k) \\
x_4(k+1) & = & (1-\frac{\pi}{N}\frac{1}{\tau_e})x_4(k)+\frac{\pi}{N}\frac{1}{\tau_e}x_3(k) \\
x_5(k+1) & = & x_4(k) \\
x_6(k+1) & = & x_5(k) \\
x_7(k+1) & = & x_6(k) \\
x_8(k+1) & = & (1-\frac{\pi}{N}\frac{1}{\tau_s})x_8(k)+\frac{\pi}{N}\frac{1}{\tau_s}x_7(k) \\
q_1(k+1) & = & q_1(k)+\frac{\pi}{N}(T_b-T_{b,ref}) \\
 & = & q_1(k)+\frac{\pi}{N}(\delta(N)-T_{b,ref}+410.86x_1(k) \\
 & & -2.98(x_3(k)-A/F_{stoic.})) \\
q_2(k+1) & = & q_2(k)+\frac{\pi}{N}(A/F_{EGO}-A/F_{stoic.}) \\
 & = & q_2(k)+\frac{\pi}{N}(x_8(k)-A/F_{stoic.})
\end{array}$$

where
τ_e : time constant of exhaust manifold (=0.15)
τ_s : time constant of EGO sensor (=0.20)

(24)

V_{L1} and V_{L2} are simply extended and replaced with

$$\begin{array}{ll}
V_{L1}(k)= & (410.86\frac{\pi}{N}x_1(k)+q_1(k)+2.98(q_2(k)+\tau_e x_4(k) \\
 & +\tau_s x_8(k)+\frac{\pi}{N}(x_5(k)+x_6(k)+x_7(k))))^2 \\
V_{L2}(k)= & (x_2(k)+K(q_2(k)+\tau_e x_4(k)+\tau_s x_8(k) \\
 & +\frac{\pi}{N}(x_3(k)+x_5(k)+x_6(k)+x_7(k))))^2
\end{array} \tag{25}$$

The same argument used with the simplified version can be repeated, and it shows that the control signals converge to

$$\begin{array}{ll}
\Delta A \longrightarrow & \frac{T_{b,ref}-\delta(N)}{410.86T} \\
\Delta F \longrightarrow & (1-K\frac{\pi}{N}\frac{T_{b,ref}-\delta(N)}{410.86T})x_2(k)+K\frac{\pi}{N}A/F_{stoic.}
\end{array} \tag{26}$$

From this, it can be shown that $x_2 \rightarrow \frac{A/F_{stoic.}}{\Delta A}$, and thus, $x_3 \rightarrow A/F_{stoic.}$. Consequently, the other states along the exhaust pipe and the EGO sensor converge to constant values because they are asymptotically stable.

4.2 Back stepping

To drive the mass air flow rate into the cylinders ($\dot{m}_{cyl}$) to the desired value (ΔA), the control law designed in the previous subsection is back stepped through the actuator dynamics [14].
The candidate Lyapunov function for back stepping is chosen to force $\dot{m}_{cyl}$ to the control signal ΔA computed in (12):

$$V_{L3}(k)=V_3^2(k)=(\alpha(k)\dot{m}_f(k)-\Delta A)^2 \tag{27}$$

The difference equation of the Lyapunov function V_{L3} is then given by

$$V_{L3}(k+1)-V_{L3}(k)=(V_3(k+1)-V_3(k))(V_3(k+1)+V_3(k))$$

where
$V_3(k+1)-V_3(k)$
$=f_1(P_m(k),\alpha(k),x_r(k),u_r(k),N)+\frac{\pi}{N\tau_a}f_2(P_m(k),N)u_c(k)$

(28)

A positive semi-definite Lyapunov function for the overall engine model can be taken as

$$V_L=V_{L1}+V_{L2}+V_{L3} \tag{29}$$

Direct calculation shows that the control law

$$\begin{array}{l}
u_c(k)=\frac{N\tau_a}{\pi f_2}(-f_1-c_3V_3(k)) \\
F_c(k)=\frac{1}{\Delta F}=\frac{1}{-K\frac{\pi}{N}(x_1(k)\alpha(k)\dot{m}_f(k)-A/F_{stoic.})+x_1(k)-c_2V_2(k)}
\end{array} \tag{30}$$

with appropriate gain c_3, makes the difference equation of Lyapunov function V_L negative semi-definite,

$$\begin{array}{l}
V_L(k+1)-V_L(k) \\
=-c_1(2-c_1)V_1^2(k)-c_2(2-c_2)V_2^2(k)-c_3(2-c_3)V_3^2(k)
\end{array} \tag{31}$$

If there were no saturation, the stability of the complete system would be guaranteed from the results of the previous subsection and the back stepping procedure. However, saturation definitely does occur and must be addressed. This is done in the next subsection.

4.3 Saturation recovery

One way to preserve stability, in the face of saturation, is to consistently force the Lyapunov difference to be negative semi-definite regardless of saturation. For this purpose, the reference signal, u_r, in (7), is used like a control input instead of the effective area of the intake valve. The case $\alpha=0$ is not considered here because it physically means that engine stops by misfire. The Lyapunov

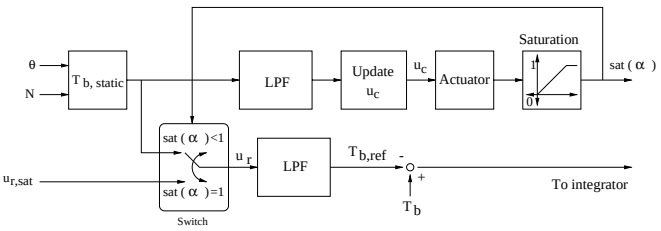

Figure 8: Diagram of reference switching structure.

function V_{L3} under saturation is equal to

$$V_{L3}(k)=V_3^2(k)=(\dot{m}_f(k)-\Delta A)^2 \tag{32}$$

The difference equation of Lyapunov function V_{L3} then becomes

$$V_{L3}(k+1)-V_{L3}(k)=(V_3(k+1)-V_3(k))(V_3(k+1)+V_3(k))$$

where
$V_3(k+1)-V_3(k)=f_3(P_m(k),x_r(k),N)-\frac{1}{410.86T}\frac{\pi}{N\tau_r}u_r(k)$

(33)

The modified reference signal ($u_r=u_{r,sat}$)

$$u_{r,sat}(k)=\frac{410.86TN\tau_r}{\pi}(f_3+c_3V_3(k)) \tag{34}$$

preserves the negative semi-definiteness of the difference equation of Lyapunov function V_L

$$V_L(k+1) - V_L(k) = -c_1(2-c_1)V_1^2(k) - c_2(2-c_2)V_2^2(k) - c_3(2-c_3)V_3^2(k) \quad (35)$$

Even when the reference signal is modified, the control signal for the intake valve effective area, u_c, is still updated by (30) so that the effective area change of the intake valve can regain control authority when the reference torque from the $T_{b,static}$ is achievable without saturation. A schematic diagram of the reference switching structure is shown in Figure 8. Through this scheme, u_c can be shown to be bounded and to converge regardless of saturation.

4.4 Observer based implementation

The above nonlinear feedback was implemented on the engine via a nonlinear observer. The specific observer used was essentially a constant gain, extended Kalman filter. In general, the stability of the resulting observer-based closed-loop system is not guaranteed, and its analysis is not carried out here. For the purposes of this paper, the stability will be "checked" via simulation along with the performance of the controller.

5 Simulations

The performance of the controller designed above was evaluated through simulations. The parameters c_1, c_2, c_3 and K were set to be 0.1, 0.1, 0.8 and 4 respectively. The time constant, τ_r, of the torque reference model was set to 0.1. $+15^\circ$ step changes were given in the primary throttle angle, from a nominal position of 5.5°; $A/F_{stoic.}$ is set to be 14.64, and the engine speed was held constant at 150 rad/sec.

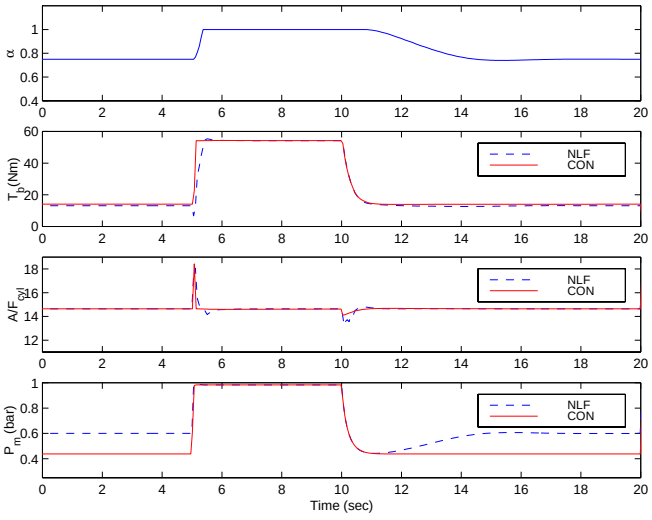

Figure 9: Simulations results with constant engine speed 150 rad/sec. NLF and CON stand for designed nonlinear feedback controller and conventional fuel PI controller, respectively.

First, the controller was simulated on the nominal model, which includes the nonlinear torque representation, (4). The torque and A/F responses were compared to the conventional engine, with fuel controlled by the standard PI controller. The results, displayed in Figure 9, show that the engine with joint air and fuel control achieves similar torque response to the conventional engine, and almost equivalent A/F performance.

Figure 9 also displays the intake manifold pressure. The possibility of controlling the cylinder air charge process has resulted in the ability to maintain a higher manifold pressure than that of the conventional engine, resulting in a potential reduction of pumping losses at low primary throttle angles. As discussed previously, this potential would be realized if the actuation were implemented with variable valve timing or height, secondary valves, or via variable cam timing, but would not be realized in the case of secondary throttles. The steady state torque value is approximately equal to that of the conventional engine, even in higher intake manifold pressure, because mass air flow into the cylinders saturates at intake manifold pressures lower than around 0.5 bar.

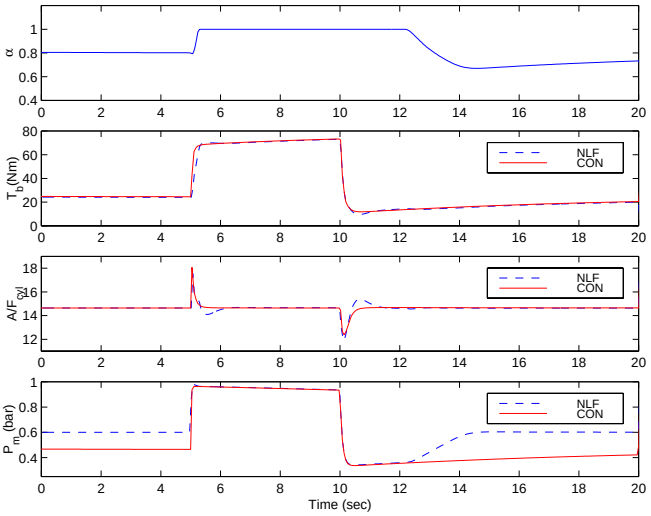

Figure 10: Simulations results with model errors. Transmission is in third gear.

In the second simulation, shown in Figure 10, errors were deliberately introduced into the simulation model. Specifically, the air flow actuator dynamics has a steady state error of 2%, and the fuel puddle dynamics developed in [4] is included in the fuel path after injection delay. In addition, the engine rotational dynamics was included, and engine speed was allowed to vary. $+15^\circ$ step changes were given in the primary throttle angle, from a nominal position of 10°. It is seen that the controller achieves comparable performance even in the presence of model errors.

In both simulations, during tip-in, saturation occurs. However, saturation is promptly recovered by the modified reference signal without any harmful effect on A/F excursions, as can be seen in Figure 9.

Appendix

Discrete-time version of Theorem 2.24 in [11]

Consider the time-invariant system

$$x(k+1) = f(x(k)) \quad \text{(i)}$$

where $x \in R^n$ and $f : R^n \to R^n$ is continuous. Let $x = 0$ be an equilibrium of (i) and let $V(x)$ be a continuous positive semidefinite

function such that $\Delta V \leq 0$. Let Z be the largest positively invariant set contained in $\{x|V(x) = 0\}$. If $x = 0$ is asymptotically stable conditionally to Z, then $x = 0$ is stable.

Proof : The proof follows closely the one given in [11], and is by contradiction. Let $x(K;x_0) := f^{(K)}(x_0)$, where $f^{(K)}$ denotes f composed with itself K-times. Suppose that $x = 0$ is unstable. Then it can be shown that for every $\varepsilon > 0$ small enough, there exist a sequence $(x_i)_{i\geq 1} \to 0$ in R^n and a sequence $(k_i)_{i\geq 1}$ in N^+ (the positive integers) such that

$$\forall k \in [0, k_i), \; ||x(k;x_i)|| < \varepsilon \quad \text{and} \quad ||x(k_i;x_i)|| \geq \varepsilon \qquad \text{(ii)}$$

Using the continuity of f and the fact that $f(0) = 0$, it can be arranged that $||x(k_i;x_i)|| = \varepsilon$, and moreover, it can be shown that $k_i \to \infty$ as $i \to \infty$. The new sequence $z_i := x(k_i;x_i)$ belongs to a compact set, and thus there exists a subsequence $z_{n_i} := x(k_{n_i};x_{n_i})$ that converges to $z \in R^n$ with $||z|| = \varepsilon$.
The next step is to construct pre-images of z with certain properties. Since $k_i \to \infty$, for every $K \in N^+$, there exists $I_K < \infty$ such that the sequence $z^K_{n_i} := x(k_{n_i} - K;x_{n_i})$, $i \geq I_N$ is well-defined. By (ii), $||z^K_{n_i}|| < \varepsilon$, and thus there exists a convergent subsequence; denote the limit by z^{-K}. By construction, $||z^{-K}|| \leq \varepsilon$. By the continuity of f, it follows that $f^{(K)}(z^{-K}) = z$. It is now shown that z and z^{-K} belong to Z. Since V is non-increasing along solutions, $V(z) = 0 \Rightarrow z \in Z$. Since V is continuous and non-increasing along solutions, $V(z) := \lim_{i\to\infty} V(x(k_{n_i};x_{n_i})) \leq \lim_{i\to\infty} V(x_{n_i}) = 0$, where the last equality used that facts that $x_{n_i} \to 0$ along with $V(0) = 0$. The same argument shows that $z^{-K} \in Z$.
In summary, it has been shown that for every $\varepsilon > 0$ and $K \in N^+$, there exist vectors $z^{-K} \in Z$ and $z \in Z$ such that

$$||z^{-K}|| \leq \varepsilon \qquad \text{(iii)}$$

$$f^{(K)}(z^{-K}) = z \qquad \text{(iv)}$$

$$||z|| = \varepsilon \qquad \text{(v)}$$

It remains to prove that (iii) - (v) cannot hold if the equilibrium $x = 0$ is asymptotically stable conditionally to Z. Because $\varepsilon > 0$ can be chosen arbitrary small, it can be assumed without loss of generality that for any initial condition $x_0 \in Z$ with $||x_0|| \leq \varepsilon = ||z||$, the solution converges to zero. So, there exists a constant $K = K(\varepsilon) > 0$, independent of x_0, such that $||x(K;x_0)|| \leq \frac{\varepsilon}{2}$. Because of (iii) - (v), one possible choice for x_0 is z^{-K}. But then $\frac{\varepsilon}{2} \geq ||x(K;z^{-K})|| = ||x(K-K;z)|| = ||z|| = \varepsilon$ which is a contradiction.

Acknowledgments

The authors thank A. Stefanopolou and J. Cook for helpful discussions. This work was supported by an NSF GOALI grant, ECS-9631237, with matching funds from Ford Motor Company.

References

[1] A. G. Stefanopoulou. Modeling and Control of Advanced Technology Engines. PhD thesis, University of Michigan, 1996.

[2] J. B. Heywood. Internal Combustion Engine. McGraw-Hill, 1988.

[3] P. R. Crossley and J. A. Cook. A Nonlinear Model for Drivetrain System Development. IEE Conference 'Control 91', Edinburgh, U.K., Volume 2, pages 921-925, IEE Conference Publication 332, March 1991.

[4] C. F. Aquino. Transient A/F Control Characteristics of the 5 Liter Central Injection Engine. SAE Paper 810494.

[5] A. L. Emtage, P. A. Lawson, M. A. Passmore, G. G. Lucas and P. L. Adcock. The Development of an Automotive Drive-By-Wire Throttle System as a Research Tool. SAE Paper 910081.

[6] M. S. Ashhab, A. G. Stefanopoulou, J. A. Cook and M. Levin. Camless Engine Control for Robust Unthrottled Operation. SAE Paper 981031.

[7] A. G. Stefanopoulou, J. W. Grizzle and J. S. Freudenburg. Engine Air-Fuel Ratio and Torque Control using Secondary Throttles. Proc. IEEE Conf. Decision and Control, Orlando, pages 2748-2753, 1994.

[8] J. A. Cook and B. K. Powell. Discrete Simplified External Linearization and Analytical Comparison of IC Engine Families. Proc. Amer. Contr. Conf., Minneapolis, pages 325-333, June 1987.

[9] S. Yurkovich and M. Simpson. Comparative Analysis for Idle Speed Control: A Crank-Angle Domain Viewpoint. Proc. Amer. Contr. Conf., New Mexico, pages 278-283, June 1997.

[10] O. Vogel, K. Roussopoulos, L. Guzzella and J. Czekaj. Variable valve timing implemented with a secondary valve on a four cylinder SI engine. 1997 Variable Valve Actuation and Power Boost SAE Special Publications, volume 1258, number 970335, pages 51-60, February, 1997.

[11] R. Sepulchre, M. Janković and P.V. Kokotović. Constructive Nonlinear Control. Springer, 1997.

[12] Eduardo D. Sontag. A 'universal' construction of Artstein's theorem on nonlinear stabilization. System & Control Letters, volume 13, pages 117-123, 1989.

[13] Pierre Bidan, Serge Boverie and Vincent Chaumerliac. Nonlinear Control of a Spark-Ignition Engine. IEEE Transactions on Control Systems Technology, volume 3, number 1, pages 4-13, March 1995.

[14] M. Krstić, I. Kanellakopoulos and P. Kokotović. Nonlinear and Adaptive Control Design. Wiley-Interscience, New York, 1995.

[15] V. Lakshmikantham and D. Trigiante. Theory of Difference Equation: Numerical Methods and Applications. Academic Press, 1988.